Turbulence Intensity Effects on Laminar Separation Bubbles Formed over an Airfoil

Mark S. Istvan,* John W. Kurelek,* and Serhiy Yarusevych†
University of Waterloo, Waterloo, Ontario N2L 3G1, Canada

DOI: 10.2514/1.J056453

The effects of freestream turbulence intensity on the mean topology and transition characteristics of laminar separation bubbles forming over the suction side of a NACA 0018 airfoil are investigated experimentally for angles of attack between 0 and 20 deg, chord Reynolds numbers between 100,000 and 200,000, and freestream turbulence intensities between 0.09 and 2.03%. The results show that increasing freestream turbulence intensity results in earlier transition and reattachment, contributing to an overall decrease in separation bubble length. At lower angles of attack, this is accompanied by a minor decrease in lift, whereas at prestall angles of attack and higher turbulence intensity levels, lift increases and stall is delayed. Spatial amplification rates of disturbances in the separated shear layer are shown to decrease at elevated levels of turbulence intensity, indicating that the earlier transition is attributed solely to the larger initial amplitude of perturbations. At elevated turbulence intensity levels, a broader range of unstable frequencies is detected in the separated shear layer, with the central frequency of the unstable band showing moderate variations with the level of freestream perturbations. The results indicate a change in the transition process at higher freestream turbulence intensity levels, indicative of bypass transition in the boundary layer. The degree of influence of freestream turbulence intensity on the separation bubble is shown to decrease as the chord Reynolds number is increased.

Nomenclature

C_l	=	sectional lift coefficient
$C_{l,\max}$	=	maximum of C_l
C_P	=	surface pressure coefficient, $(P - P_0)/q_0$
c	=	airfoil chord length
d	=	turbulence-generating grid element size
E_{pp}	=	energy spectrum of p
E_{uu}	=	energy spectrum of u
f	=	frequency
f_0	=	central disturbance frequency
ℓ_b	=	separation bubble length, $x_R - x_S$
M	=	turbulence grid mesh spacing
P	=	mean surface pressure
P_0	=	mean freestream static pressure
p	=	fluctuating surface pressure
p'	=	root mean square of p
$p'_{\max}$	=	maximum of p'
q_0	=	freestream dynamic pressure, $0.5\rho U_0^2$
Re_c	=	Reynolds number based on airfoil chord length, $U_0 c/\nu$
Tu	=	freestream turbulence intensity, u'/U_0
U	=	freestream velocity
U_0	=	mean freestream velocity
u	=	fluctuating component of U
u'	=	root mean square of u
X	=	streamwise coordinate relative to the turbulence-generating grids
x, y, z	=	chordwise, vertical, and spanwise coordinates relative to the midspan of airfoil leading edge
x_S, x_T, x_R	=	chordwise locations of mean separation, transition, and reattachment
α	=	airfoil angle of attack
β	=	turbulence grid porosity, $(1 - d/M)^2$
Δf	=	unstable frequency band
Λ	=	integral length scale
ν	=	kinematic viscosity of air
ρ	=	density of air
σ	=	spatial amplification factor
$\sigma_{\max}$	=	maximum of σ

I. Introduction

AIRFOILS operating at low chord Reynolds numbers, characterized by values typically less than 500,000, generally have a decreased aerodynamic performance as compared with those operating at higher chord Reynolds numbers [1,2]. As such, research efforts over the last several decades have focused on low Reynolds number airfoil flows, with the aim of identifying performance improvements for applications such as unmanned aerial vehicles, small to medium sized wind turbines, and compressor and turbine blades [1,3–5]. The main impediment to airfoil performance at low Re_c is laminar boundary-layer separation on the suction side of the airfoil. Following separation, if the flow remains detached the airfoil is stalled and experiences high drag and low lift [1]. However, if the flow reattaches downstream of separation, a laminar separation bubble (LSB) is formed [6,7] and performance improves with respect to the stalled case. Early experimental studies [6–8] established a description of the time-averaged topology of LSBs, which is depicted in Fig. 1.

LSBs formed over airfoils [10–13], as well as flat plates with an imposed adverse pressure gradient [14–17], have been studied experimentally and numerically. A parametric study of LSBs formed over a NACA 0018 airfoil conducted by Boutilier and Yarusevych [9] summarizes generally accepted trends for Reynolds number and angle-of-attack effects on the time-averaged bubble characteristics. It has been established that LSBs form earlier upstream and decrease in length with increasing angle of attack or chord Reynolds number. The laminar-to-turbulent transition process in separation bubbles has a significant influence on LSB characteristics and, as such, has been studied extensively experimentally [11,15,18,19] and numerically [20–23]. The transition process is initiated by the amplification of small-amplitude disturbances that originate from the freestream through the receptivity process [24]. The disturbances within an unstable wave packet undergo near exponential amplification dominated by the normal

Presented as Paper 2016-3946 at the 46th Fluid Dynamics Conference, Washington, D.C., 13–17 June 2016; received 19 June 2017; revision received 13 October 2017; accepted for publication 26 October 2017; published online 13 December 2017.

*Graduate Student, Mechanical and Mechatronics Engineering, 200 University Avenue West. Student Member AIAA.

†Associate Professor, Mechanical and Mechatronics Engineering, 200 University Avenue West. Senior Member AIAA.

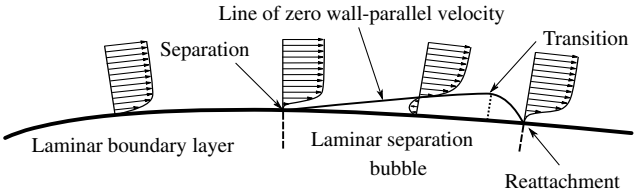

Fig. 1 Time-averaged laminar separation bubble (after Boutilier and Yarusevych [9]).

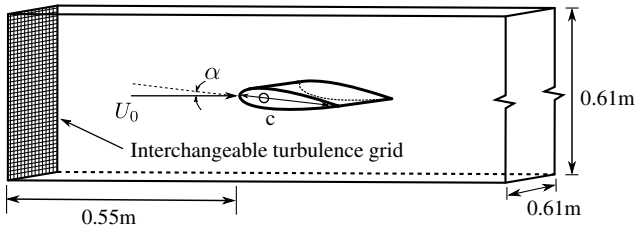

Fig. 2 Experimental arrangement.

modes in the separated shear layer [15,25], with the process being modeled well by linear stability theory [18,21]. As the disturbances reach significant amplitudes, nonlinear interactions begin to occur [25], marking the later stages of transition. The formation of coherent structures has been observed during the later stages of transition, where the separated shear layer rolls up into vortices that are shed at the frequency of the most amplified disturbances [11,13,19,26]. These structures effectively govern the flow development in the aft portion of the bubble [11,19,26,27].

Transition in the separated shear layer is inherently sensitive to small-amplitude environmental disturbances and, therefore, significant effects of freestream turbulence intensity on the transition process have been noted in several investigations [11,22,28,29]. At low levels of Tu, the separated shear layer rolls up into large-scale vortices in the aft portion of the bubble [11,22,29]. At elevated levels of Tu, weaker shear layer roll-up is observed [22,23,29]. This may be a consequence of the reduction in the size of the separation bubble, and thus roll up occurring closer to the wall, and/or interaction of spanwise rollers with streamwise structures that have been observed to form in the boundary layer upstream of separation [22].

Previous investigations have examined the effect of Tu on the performance of airfoils [30–32] and, more specifically, on suction-side LSB characteristics [10,28,33]. At elevated levels of Tu, an increase in the lift coefficient near stall has been observed [30,32] as well as a delay in the stall angle [31]. Mueller et al. [30] found that the hysteretic dependence of lift on the direction of approach to the stall angle is reduced at elevated levels of Tu. Increasing levels of Tu have also been shown to reduce the length of the LSB [10,28,33,34]. Ol et al. [33] demonstrated that nominally identical experiments performed in different facilities can produce notably different results. For example, they found that locations of mean separation, transition, and reattachment varied by as much as $0.15c$, $0.10c$, and $0.05c$, respectively. These discrepancies are attributed to differences in the freestream characteristics in the three facilities (i.e., turbulence intensity, length scales, and disturbance spectrum), of which only turbulence intensities were reported and varied by as much as 0.1% between the facilities. Through a combination of experiments and numerical simulations of an LSB formed over the suction side of an SD7003 airfoil, Olson et al. [28] found that increasing Tu from 0.3 to 0.9% led to a downstream shift of $0.03c$ in the location of mean separation and an upstream shift of $0.12c$ in the location of mean reattachment. These modifications to mean bubble topology highlight the challenges in comparing experimental results obtained at different freestream conditions. The studies summarized here, and the majority found in literature [10,28,30–34], have focused on the effects of freestream turbulence intensity on time-averaged LSB characteristics and/or airfoil performance, whereas the associated changes in separation bubble dynamics remain to be addressed. Moreover, the influence of turbulence intensity has been typically considered for a specific set of experimental conditions (i.e., a fixed angle of attack and Reynolds number), and thus added insight is required into the interdependence between Reynolds number, angle of attack, and freestream turbulence intensity level.

The purpose of the present investigation is to investigate the effects of freestream turbulence intensity on laminar separation bubbles formed over the suction side of a NACA 0018 airfoil over a relatively wide range of angles of attack ($0 \leq \alpha \leq 20$ deg), Reynolds numbers ($100{,}000 \leq Re_c \leq 200{,}000$), and levels of freestream turbulence intensity ($0.09 \leq Tu \leq 2.03\%$). Mean surface pressure measurements are used to identify the location of the separated flow region, quantify its extent, and determine sectional lift. Fluctuating surface pressure measurements are used to provide insight into the transition process and gain insight into the observed changes in mean separation bubble characteristics.

II. Experimental Setup

All experiments were performed in the closed-loop wind tunnel located in the Fluid Mechanics Research Laboratory at the University of Waterloo. The test section of the tunnel is 0.61 m wide by 0.61 m high and 2.4 m long. The flow is conditioned by aluminum honeycomb and a set of five screens upstream of a 9:1 contraction, resulting in a freestream turbulence intensity of 0.1% over the investigated Reynolds number range. The freestream velocity was set based on the static pressure drop measured across the tunnel contraction, which was calibrated against a Pitot-static tube in the empty test section. The associated uncertainty in U_0 is approximately 2%.

The freestream turbulence intensity was elevated above the baseline level by placing turbulence-generating grids just upstream of the test section inlet, as depicted in Fig. 2. The characteristic dimensions of the turbulence-generating grids are provided in Table 1. The relationship between the contraction pressure drop and the test section velocity was established for each turbulence-generating grid. Square grids of elements are commonly used as a passive method of generating nearly homogeneous and isotropic freestream turbulence [35–37]. In this investigation, the first three grids (i.e., cases 2–4 in Table 1) are woven wire mesh screens, whereas the final grid is a square array of rectangular elements. In considering the downstream distance of the airfoil from the grids X relative to the mesh size M, Batchelor and Townsend [38] suggest that the region of developing turbulence is located within $X/M \leq 20$. In their review, Laws and Livesey [37] suggest that this region extends to $X/M = 40$. For the present investigation, the airfoil leading edge is located within $38 \lesssim X/M \lesssim 820$, depending on the grid, and is thus assumed to be subjected to nearly homogeneous and isotropic freestream turbulence.

Freestream turbulence intensities were measured by means of hot-wire anemometry in the empty test section at the location corresponding to the midspan and leading edge of the airfoil at zero angle of attack. Measurements were conducted using a normal Dantec 55P11 probe connected to a Dantec Streamline Constant Temperature Anemometry system. The probe was calibrated in situ against a Pitot-static probe positioned approximately 3 cm below the hot-wire probe. A total of 2^{23} samples were recorded at a rate of 100 kHz, with the signal low-pass filtered at 50 kHz using an analog filter. The turbulence intensity $Tu = u'/U_0$ was then computed from the low-pass-filtered signal. Integral length scales were calculated from the integral of an exponential curve fit to the autocorrelation function of the velocity fluctuations with the use of Taylor's hypothesis [39]. The obtained turbulence intensities and integral length scales are presented in Table 2. Spectra of the hot-wire signals were computed using Welch's

Table 1 Turbulence-generating grid parameters

Case	d, mm	M, mm	β, %
1) No screen	— —	— —	— —
2) Fine screen	0.11	0.67	70
3) Medium screen	0.26	1.48	68
4) Coarse screen	0.48	2.19	61
5) Grid	1.72	14.32	77

Table 2 Summary of investigated flow conditions

	$Re_c = 100{,}000$		150,000		200,000	
Case	Tu, %	Λ, mm	Tu, %	Λ, mm	Tu, %	Λ, mm
1	0.10	74.33	0.10	88.31	0.09	95.51
2	0.24	2.88	0.25	2.47	0.26	1.91
3	0.37	3.30	0.37	2.61	0.35	2.21
4	0.51	3.61	0.54	2.96	0.60	2.69
5	1.94	6.03	1.90	5.23	2.03	4.73

method [40], with a resulting frequency resolution of 0.8 Hz. The representative spectra in Fig. 3 indicate that all turbulence-generating grids increased velocity fluctuations over a broad range of frequencies, resulting in the overall increase in Tu level.

Experiments were performed using an aluminum NACA 0018 airfoil with a chord length and span of 0.2 and 0.61 m, respectively. The airfoil is equipped with 65 streamwise pressure taps, of 0.4 mm diameter, distributed in two staggered rows at the midspan (Fig. 4). The model is also equipped with an array of 22 microphones embedded under 0.8 mm ports in two staggered rows centered at $z/c \approx -0.2$ on the suction side. Before the experiments, all microphones were calibrated in their model arrangement against a reference Brüel and Kjær 4192 microphone over a range of frequencies from 100 to 5000 Hz. Additional details about the airfoil model and microphone frequency response are provided by Gerakopulos and Yarusevych [41]. To minimize end effects, the airfoil model was fitted with circular end plates, $2.25c$ in diameter, with a spanwise spacing of $2c$ as per the recommendation of Boutilier and Yarusevych [42]. For the investigated angles of attack, the blockage ratio was within the range of 7.4–12.8%. It has been shown that blockage corrections perform adequately for angles of attack below the stall angle [42]; however, their performance deteriorates substantially at poststall angles of attack. Therefore, for consistency, the data are presented

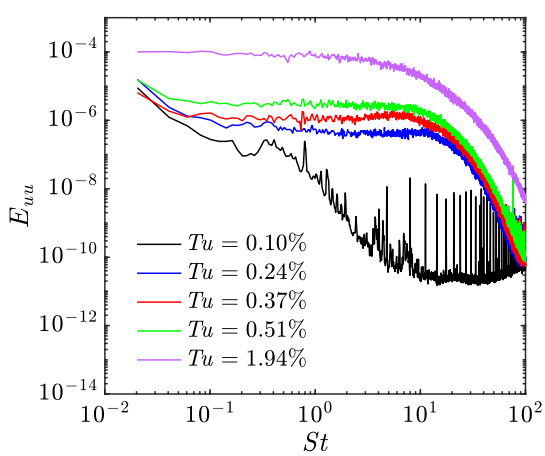

Fig. 3 Spectra of freestream velocity fluctuations at $Re_c = 100{,}000$.

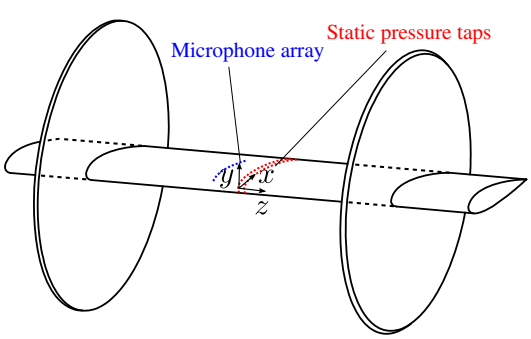

Fig. 4 Airfoil model.

without any blockage corrections applied. A digital protractor affixed to the airfoil axis of rotation was used to set the angle of attack to within 0.1 deg relative to the aerodynamic zero reference.

Mean surface pressure measurements were performed by mechanically multiplexing the pressure taps through a Scanivalve unit to two Setra 239 differential pressure transducers. Measurements were referenced against a freestream static pressure tap located in the floor of the test section approximately $2c$ upstream of the airfoil. For each pressure tap, the pressure in the tubing was given at least 25 s to equalize after the multiplexer was indexed. Then, 10^4 samples were acquired at 1 kHz using a National Instruments USB-6259 data acquisition unit. The transducers had full-scale ranges of ± 600 and ± 250 Pa to measure the suction- and pressure-side pressure distributions, respectively, resulting in uncertainties of 6 and 5% of the freestream dynamic pressure, respectively. To measure fluctuating surface pressures, the microphone signals were sampled simultaneously at 40 kHz using two National Instruments 9220 data acquisition modules for a total of 2^{20} samples.

III. Results

Measurements were performed for $0 \le \alpha \le 20$ deg, $100{,}000 \le Re_c \le 200{,}000$, and $0.09 \le Tu \le 2.03\%$. Because of the large test matrix, a select portion of the results is presented to highlight the main trends and the associated flow characteristics. First, the effects of Tu and Re_c on airfoil lift are examined. Then, the effects on mean separation bubble topology are evaluated and linked to the observed changes in airfoil lift. Finally, the associated changes in separated shear layer disturbance evolution are examined.

A. Airfoil Lift

The effects of freestream turbulence intensity on the flow over the airfoil are first assessed by means of the sectional lift coefficient, calculated by numerically integrating the measured mean surface pressure distributions. The results are presented in Fig. 5 for each of the three chord Reynolds numbers investigated. For the baseline case, the data are in good agreement with previous investigations on a NACA 0018 airfoil [9,43,44]. Examining the results for all the cases, the following distinct regions can be identified in Fig. 5: 1) "low angles of attack," $\alpha \lesssim 6$ deg, where C_l increases approximately linearly with angle of attack; 2) "prestall angles of attack," from $\alpha \approx 7$ deg to stall, where increases in C_l with α gradually become less significant; and 3) "poststall angles of attack," where C_l begins to recover after the sharp drop at stall.

At low angles of attack, there is no significant variation in C_l with increasing Tu. For a given Tu level, the rate of increase in C_l with angle of attack increases as the angle of attack increases, similar to the trend reported by Boutilier and Yarusevych [9]. As the angle of attack approaches the prestall range ($\alpha \approx 6$ deg), marginally higher lift is generated at lower Tu levels. This occurs at higher angles of attack with increasing Reynolds numbers, as the onset of the prestall range shifts to higher incidences, namely, to $\alpha \approx 6$, 7, and 8 deg, for $Re_c = 100{,}000$; 150,000; and 200,000, respectively. At prestall angles of attack, the lift curves show significant differences based on Tu level. Here, as the level of Tu is increased, the local lift slope is increased and, on the average, higher lift is generated at a given angle of attack. However, this effect decreases as Tu or Re_c is increased. For example, at $Re_c = 100{,}000$ (Fig. 5a), the slope of C_l with respect to α increases significantly when Tu is increased from 0.10 to 0.24%, but the subsequent increases in Tu result in progressively smaller changes in sectional lift. Similarly, as the Reynolds number increases to $Re_c = 200{,}000$ (Fig. 5c), the slopes of C_l with respect to α are approximately equal for all levels of Tu investigated, and the relative effect of increasing Tu on the lift coefficient diminishes.

The results in Fig. 5 demonstrate that stall tends to be delayed at higher Tu levels, with the effect saturating at higher levels of Tu and higher Re_c. For example, at $Re_c = 100{,}000$ (Fig. 5a) and the baseline level of Tu, the airfoil stalls at $\alpha = 14$ deg. The stall is delayed until $\alpha = 16$ deg at $Tu = 0.24\%$ and $\alpha = 17$ deg for all further increases in Tu. At $Re_c = 150{,}000$ (Fig. 5b), the stall angle is delayed from $\alpha = 16$ to 17 deg for all increases in Tu above 0.10%. At $Re_c = 200{,}000$ (Fig. 5c), the effect of Tu on the stall angle is

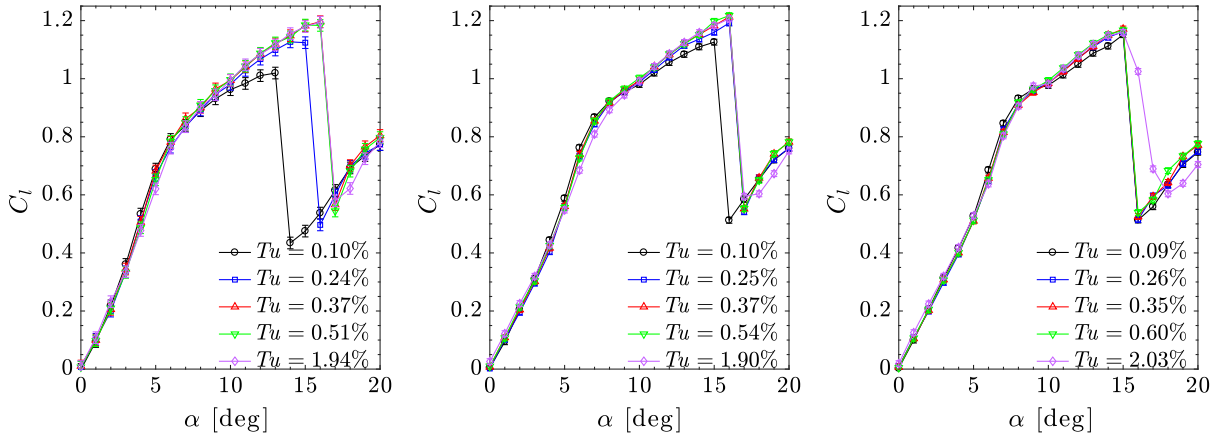

a) Re_c = 100,000 b) Re_c = 150,000 c) Re_c = 200,000

Fig. 5 Sectional lift coefficients.

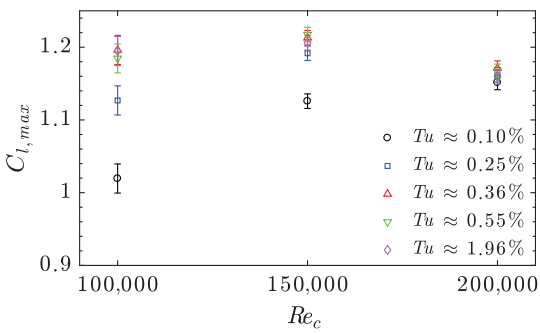

Fig. 6 Maximum sectional lift coefficients.

within the resolution of the test matrix (i.e., 1 deg) and the airfoil stalls at $\alpha \approx 16$ deg for all Tu levels. At poststall angles of attack, C_l increases at a similar rate for all Tu levels for a given chord Reynolds number. For $Re_c = 200{,}000$ and $Tu = 2.03\%$, the stall is more gradual, with lift decreasing for $16 < \alpha \leq 18$ deg. This result is similar to the findings of Cao et al. [31], who reported a more gradual decrease in the lift of an S1223 airfoil at a high Tu level. An analysis of mean and fluctuating surface pressure distributions indicate that this can be attributed to bistable oscillations between an attached and stalled state for these flow conditions.

A summary of the effects of Tu and Re_c on maximum lift coefficients is shown in Fig. 6. In general, increases in either Tu or Re_c result in an increase in $C_{l,\max}$. For example, at $Re_c = 100{,}000$, the lift coefficient is increased by approximately 17% by increasing Tu from the baseline level to the highest level investigated. Similarly, at the baseline level of Tu, $C_{l,\max}$ is increased by approximately 10 and 13% by increasing Re_c from 100,000 to 150,000 and 200,000, respectively. As noted in the previous discussions, when either Tu or Re_c are increased, the effect of the other parameter is reduced. For example, at $Re_c = 200{,}000$, $C_{l,\max}$ is increased by approximately 1% by increasing Tu from the baseline level to the highest level investigated as compared with approximately 17% at $Re_c = 100{,}000$. At all elevated levels of Tu (i.e., $Tu > 0.10\%$), $C_{l,\max}$ decreases as Re_c is increased from 150,000 to 200,000. This is due to the delay in the stall angle with increasing Tu at $Re_c = 150{,}000$ (Fig. 5b), whereas Tu has no discernible effect on stall for $Re_c = 200{,}000$ (Fig. 5c). The result is higher overall $C_{l,\max}$ values for $Re_c = 150{,}000$ as compared with $Re_c = 200{,}000$ at the elevated Tu levels. This is noteworthy because it indicates that the generally understood trend of increasing C_l with increasing Re_c for low Reynolds number airfoil flows [9] can be altered by Tu effects.

B. Surface Pressure Distributions and Mean Bubble Topology

Surface pressure distributions over the suction and pressure sides of the airfoil are presented in Fig. 7 for selected angles of attack and all Reynolds numbers investigated. Such distributions are commonly used to identify the presence and extent of a laminar separation bubble, characterized by a region of nearly constant surface pressure downstream of the suction peak [7,10]. The results show that, below the stall angle of attack (Figs. 7a–7i), separation bubbles can be identified over the suction side of the airfoil in the range of $0.1 \lesssim x/c \lesssim 0.7$, except for the case of low angles of attack at the largest Tu level investigated, for which separation bubbles cannot be detected. Beyond the stall angle, the surface pressure distributions show nearly constant pressure over the majority of the suction surface (Figs. 7j–7l). Throughout Fig. 7, marginal differences in the pressure-side C_P distributions are seen across the turbulence intensities and Reynolds numbers investigated, and therefore the focus will be on the suction-side results.

For the cases where a separation bubble forms on the suction side, the beginning of the observed pressure plateau corresponds to the location of mean flow separation x_S, whereas a subsequent region of rapid pressure recovery indicates the aft portion of the separation bubble. The onset of the rapid pressure recovery roughly corresponds to the location of mean flow transition x_T, whereas the end of this region corresponds to mean flow reattachment x_R [6,10]. It should be noted that transition occurs over a region and not a single location in space; however, a concept of a mean transition "location" is often used and is defined by the onset of rapid surface pressure recovery starting approximately at the location of the maximum bubble height [18]. The mean separation, transition, and reattachment locations were estimated in the present study using the method discussed by Boutilier and Yarusevych ([9] Fig. 5). The results are summarized in Fig. 8, where the separation, transition, and reattachment points are plotted, whereas the length of the separation bubble is shown in Fig. 9.

At low angles of attack, the separation location rapidly advances upstream as the angle of attack is increased (Fig. 8), but the overall length of the separation bubble does not change substantially for $\alpha \lesssim 4$ deg (Fig. 9). Increasing Tu leads to an overall decrease in bubble size (Fig. 9), which is attributed primarily to the earlier onset of transition and, consequently, earlier mean reattachment (Fig. 9). This is reflected in the upstream advancement of the rapid pressure recovery region seen in the insets of Figs. 7a–7c. For the highest Tu level investigated, separation appears to be suppressed on the suction side, with no evidence of a separation bubble observed in the surface pressure distributions in Figs. 7b and 7c, whereas a separation bubble is still identifiable in Fig. 7a, but not at lower angles of attack. The net reduction in bubble length with increasing Tu is particularly significant at the lower Reynolds numbers. At $Re_c = 100{,}000$ and $\alpha = 4$ deg, ℓ_b is reduced by approximately 14 and 37% by increasing Tu from the baseline level to 0.24 and 1.94%, respectively. The observed reduction in bubble length is similar to that noted by Olson et al. [28] for an SD7003 airfoil at $20{,}000 \leq Re_c \leq 40{,}000$ and

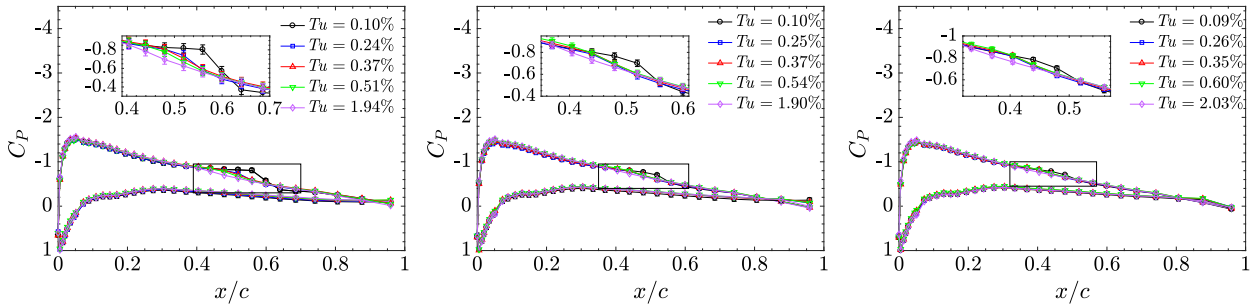

a) $\alpha = 4$ deg, $Re_c = 100{,}000$

b) $\alpha = 4$ deg, $Re_c = 150{,}000$

c) $\alpha = 4$ deg, $Re_c = 200{,}000$

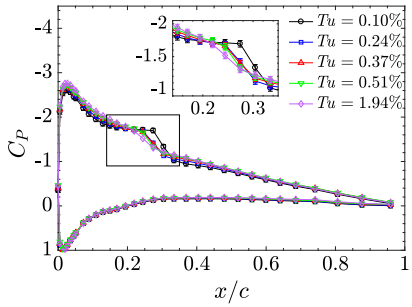

d) $\alpha = 8$ deg, $Re_c = 100{,}000$

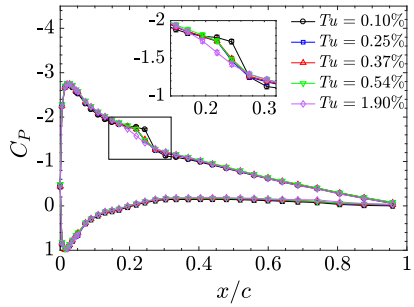

e) $\alpha = 8$ deg, $Re_c = 150{,}000$

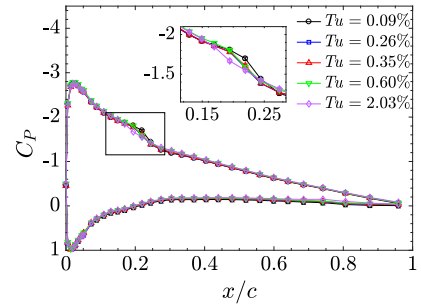

f) $\alpha = 8$ deg, $Re_c = 200{,}000$

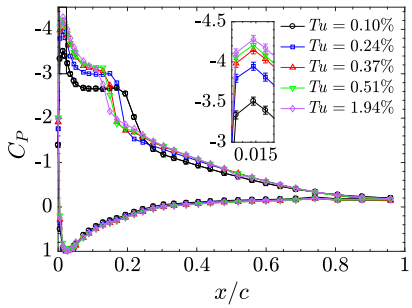

g) $\alpha = 13$ deg, $Re_c = 100{,}000$

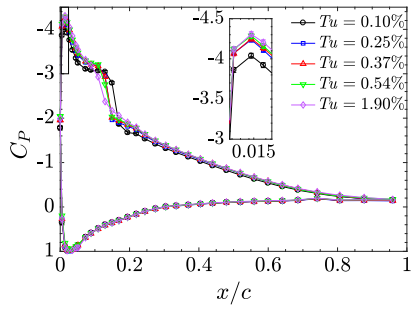

h) $\alpha = 13$ deg, $Re_c = 150{,}000$

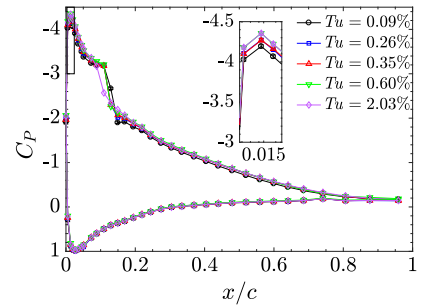

i) $\alpha = 13$ deg, $Re_c = 200{,}000$

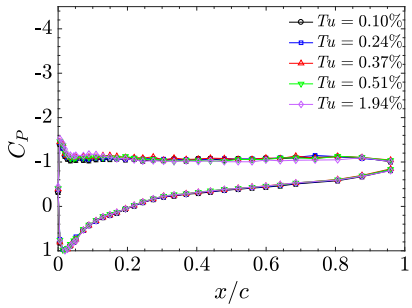

j) $\alpha = 18$ deg, $Re_c = 100{,}000$

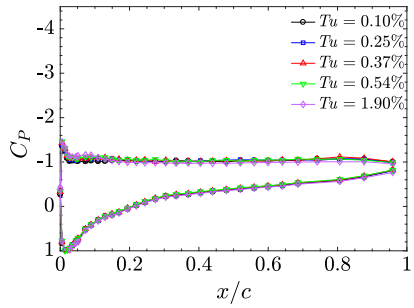

k) $\alpha = 18$ deg, $Re_c = 150{,}000$

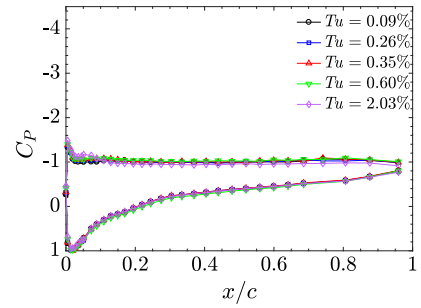

l) $\alpha = 18$ deg, $Re_c = 200{,}000$

Fig. 7 Mean surface pressure distributions. Error bars are shown in inset plots.

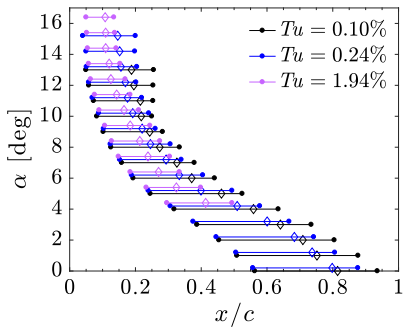

a) $Re_c = 100{,}000$

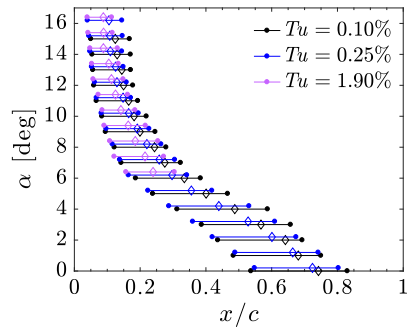

b) $Re_c = 150{,}000$

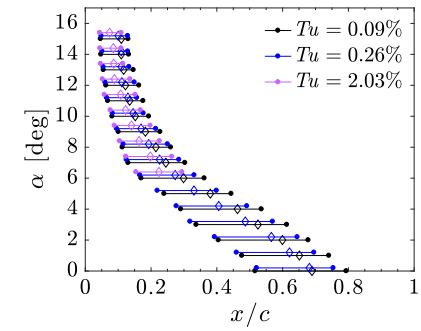

c) $Re_c = 200{,}000$

Fig. 8 Summary of mean bubble topology. Filled circles represent mean separation and reattachment locations. Diamond markers represent mean transition. Plots at equal angles of attack are offset slightly in the vertical direction for clarity. Uncertainties are approximately equal to the width of the diamond markers.

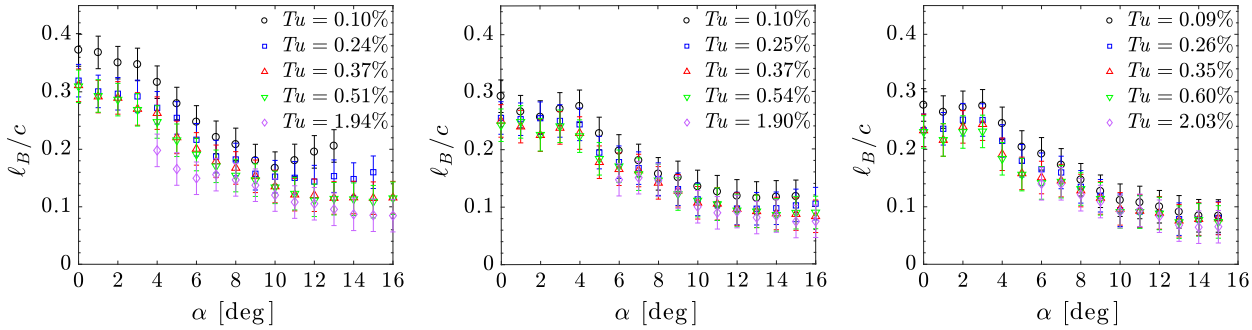

a) Re_c = 100,000 **b) Re_c = 150,000** **c) Re_c = 200,000**

Fig. 9 Mean separation bubble length.

comparable angles of attack. In their work, an increase in Tu from 0.3 to 0.9% produced a reduction of 35% in the separation bubble length. Olson et al. [28] also observed a small downstream shift in the location of mean separation with increasing Tu using estimates from molecular tagging velocimetry measurements. However, such changes in the mean separation location fall within the experimental uncertainty of the present investigation and therefore cannot be quantified. The results in Figs. 8 and 9 show that the effect of Tu on the size and position of the separation bubble become less pronounced as the Reynolds number is increased, consistent with the results in Fig. 5. At low angles of attack, the separation bubble forms over the aft portion of the airfoil (Fig. 8), substantially downstream of the suction peak (Figs. 7a–7c). Thus, the decreases in bubble size at higher Tu levels do not have any appreciable effect on the magnitude of the suction peak (Figs. 7a–7c). However, the reduction in local suction associated with the pressure plateau produced by the bubble leads to a slight reduction in lift as seen in Fig. 5 for $3 \lesssim \alpha \lesssim 7$ deg for $Re_c = 100{,}000$, and $5 \lesssim \alpha \lesssim 8$ deg for $Re_c = 150{,}000$ and 200,000.

As the angle of attack is increased above $\alpha \approx 4$ deg, the separation bubble on the suction side of the airfoil continues to move upstream (Fig. 8), but at a reduced rate, consistent with the trend reported by Boutilier and Yarusevych [9]. At the same time, the length of the separation bubble decreases rapidly (Fig. 9) due to the rapid upstream advancement of the mean transition and reattachment locations (Fig. 8). Because of the upstream motion of the bubble, its effect on the suction peak becomes more pronounced with increasing angle of attack. This can be seen from the pressure distributions in Figs. 7d–7f and Figs. 7g–7i for $\alpha = 8$ and 13 deg, respectively. Increasing Tu prompts earlier transition (Fig. 8) and reduces the size of the separation bubble, thereby enhancing the magnitude of the suction peak (Figs. 7d–7i). For example, at $Re_c = 100{,}000$ and $\alpha = 8$ deg (Fig. 7d), the magnitude of the suction peak is increased by 6% when Tu is increased from 0.10 to 1.94%. In contrast, at $Re_c = 100{,}000$ and $\alpha = 13$ deg (Fig. 7g), the magnitude of the suction peak is increased by 22% by increasing Tu from 0.10 to 1.94%, thus highlighting the increasing effect with increasing angle of attack. As a consequence, increasing Tu leads to the overall increase in C_l at prestall angles of attack (Fig. 5a). A similar increase in the magnitude of the suction peak with increasing Tu is also seen in the results of O'Meara and Mueller [10] for prestall angles of attack. As Re_c is increased, the relative effect of the Tu level on the suction peak magnitude gradually becomes less significant due to the smaller bubble that forms at the baseline level of Tu. As a consequence, the same increase in Tu level at higher Reynolds numbers leads to a less significant increase in C_l at a given prestall angle of attack (Fig. 5).

As the angle of attack is increased toward the stall angle, the rate of upstream shift in the separation bubble location decreases significantly (Fig. 8) and the rate of decrease in the bubble size diminishes (Fig. 9). At the lower Reynolds numbers, the size of the bubble increases just before stall. This effect is more pronounced for $Re_c = 100{,}000$ in Fig. 9a for angles of attack above 10 deg, where the separation bubble begins to lengthen at the baseline level of Tu. For these conditions, the chordwise distance between the mean separation and transition points remains roughly constant (Fig. 8a), whereas the distance between mean transition and reattachment increases with increasing angle of attack. A similar trend was observed in previous experiments [10] and is a precursor to bubble bursting and stall [7]. When the freestream turbulence intensity level or Reynolds number is increased, the bubble size is decreased, but the relative effect of these parameters diminishes. Beyond stall, the effect of Tu level on the mean surface pressure distribution becomes largely confined to the first 15% of the chord length, in the immediate vicinity of the suction peak (Figs. 7j–7l). However, the associated changes in surface pressure distribution do not result in appreciable changes in lift at poststall angles (Fig. 5), with the exception of the differences in stall behavior at $Re_c = 200{,}000$ highlighted earlier for the highest Tu level investigated.

The relation between the effects of freestream turbulence intensity on the mean separation bubble characteristics and the consequent changes in airfoil lift can be summarized as follows. First, for all cases examined, increasing the level of Tu leads to a reduction in the length of the suction-side separation bubble (Fig. 9), as a result of an upstream shift in mean transition and reattachment (Fig. 8). This effect decreases as the chord Reynolds number is increased. At small angles of attack, longer bubbles form over the aft portion of the suction surface relatively far downstream from the suction peak. When Tu is increased, the decrease in separation bubble length does not affect the suction peak but leads to a decrease in local suction at the location of the bubble, hence producing a minor decrease in lift (Fig. 5). At larger angles of attack, the separation bubble forms closer to the suction peak, causing a notable loss in maximum suction. As the level of Tu is increased and the bubble shrinks, the adverse influence on the suction peak is reduced and lift increases. Hence, for large prestall angles of attack where the bubble forms near the suction peak, smaller bubbles attained at high levels of Tu lead to higher lift coefficients, whereas at low angles of attack ($3 \lesssim \alpha \lesssim 7$ deg for $Re_c = 100{,}000$ and $5 \lesssim \alpha \lesssim 8$ deg for $Re_c = 150{,}000$ and 200,000), larger bubbles forming at low levels of Tu lead to higher lift coefficients. At moderate angles of attack ($7 \lesssim \alpha \lesssim 10$ deg for $Re_c = 100{,}000$ and $8 \lesssim \alpha \lesssim 11$ deg for $Re_c = 150{,}000$ and 200,000), there is a balance between these competing effects, with the main determining factors being the relative size of the separation bubble and its proximity to the suction peak.

C. Reynolds Number Effects

This section provides a brief characterization of the effect of Reynolds number on airfoil lift and the underlying changes to the mean separation bubble characteristics at different levels of freestream turbulence intensity. The results are presented for the baseline case and two elevated Tu levels (cases 1, 2, and 5 in Table 2). Although freestream turbulence intensity varies slightly with Re_c for a given screen (Table 2), the averaged levels of Tu across the investigated Reynolds numbers are used to refer to the data corresponding to a given screen configuration, namely, $Tu \approx 0.10$, 0.25, and 1.96%. Figure 10 highlights the effect of Reynolds number on lift coefficient. At a given level of Tu, increasing the Reynolds number causes a small decrease in lift at low angles of attack. At higher angles of attack at the baseline Tu level, the lift is increased with increasing Reynolds number, a trend similar to that reported by Boutilier and Yarusevych [9] in a low-disturbance

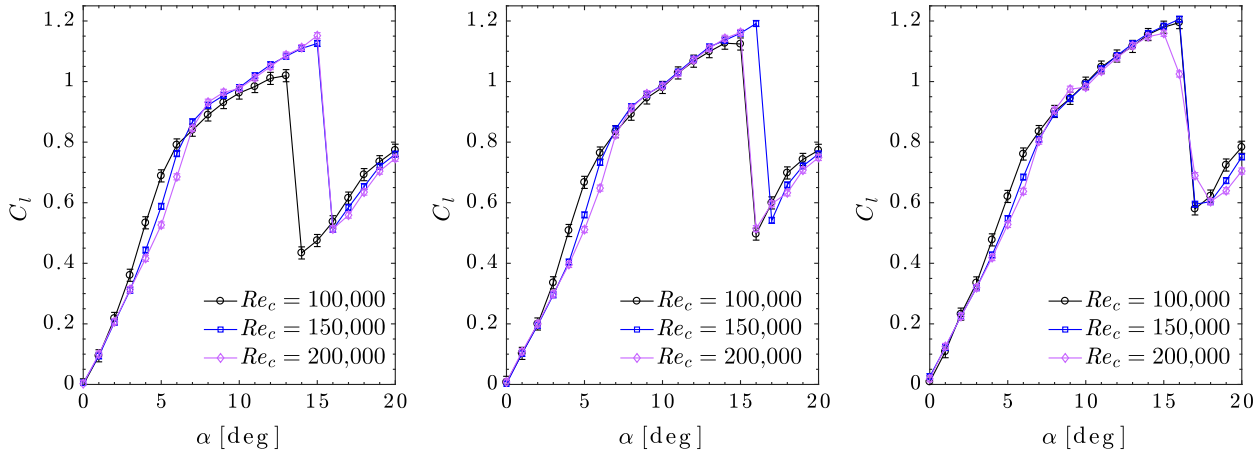

a) $Tu \approx 0.10\%$ b) $Tu \approx 0.25\%$ c) $Tu \approx 1.96\%$

Fig. 10 Effect of Reynolds number on sectional lift coefficients.

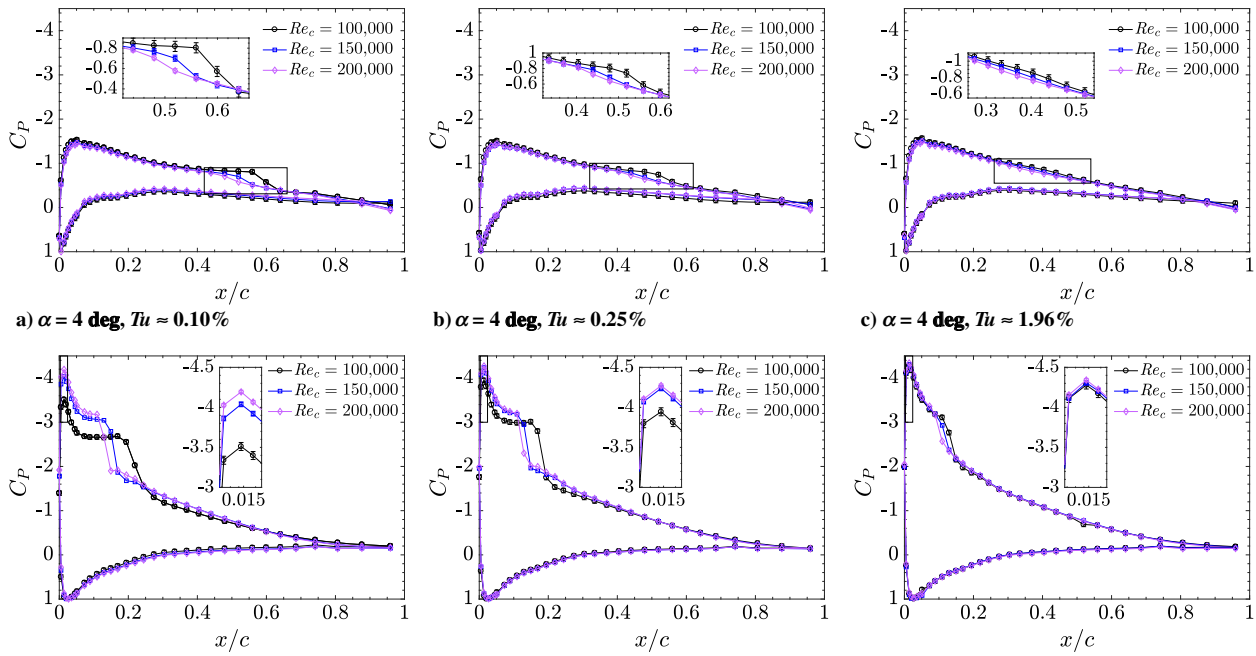

a) $\alpha = 4$ deg, $Tu \approx 0.10\%$ b) $\alpha = 4$ deg, $Tu \approx 0.25\%$ c) $\alpha = 4$ deg, $Tu \approx 1.96\%$

d) $\alpha = 13$ deg, $Tu \approx 0.10\%$ e) $\alpha = 13$ deg, $Tu \approx 0.25\%$ f) $\alpha = 13$ deg, $Tu \approx 1.96\%$

Fig. 11 Effect of Reynolds number on mean surface pressure distributions. Error bars are shown in inset plots.

environment. However, this effect diminishes at the higher levels of freestream turbulence intensity. Comparing Figs. 5 and 10, it can be seen that similar changes in lift are produced by either increasing the Reynolds number or Tu within the same ranges of angle of attack.

The effect of Reynolds number on airfoil lift is related to the underlying changes to the separation bubble characteristics on the suction side. This is illustrated in Figs. 11–13. Figure 11 shows sample surface pressure distributions for low ($\alpha = 4$ deg) and prestall ($\alpha = 13$ deg) angles of attack, whereas Figs. 12 and 13 illustrate the effect of Reynolds number on the location and length of the separation bubbles. At the baseline level of Tu, the bubble moves upstream (Fig. 12a) and decreases in length (Fig. 13a) as the Reynolds number is increased. The latter is attributed primarily to the upstream movement of transition and, hence, reattachment (Fig. 12a), consistent with the results of previous investigations [9,43]. At elevated freestream turbulence levels, similar trends are observed in Figs. 12b and 12c and Figs. 13b and 13c; however, the same increases in Re_c result in less significant changes in bubble position and length.

It can be seen from the pressure distributions in Figs. 11a–11c that the formation of the separation bubble at lower angles of attack has no significant effect on maximum suction. Increasing the Reynolds number reduces the size of the bubble and leads to a small decrease in average suction, reflected in a minor decrease in lift (Fig. 10). For prestall angles of attack (Figs. 11d–11f), the magnitude of the suction peak is affected significantly by the proximity of the separation bubble, and so the reduction in the size of the separated flow region at higher Reynolds numbers leads to a notable increase in maximum suction and a net increase in lift (Fig. 10). From a comparison of Figs. 7 and 11, it is evident that increasing either Tu or Re_c produces similar changes in the mean surface pressure distributions. Moreover, the influence of either parameter on the mean flow is reduced as the other is increased because both affect the length of the separation bubble. Comparing the effect of these parameters on mean surface pressure distributions, O'Meara and Mueller [10] noted that the effect of increasing Tu is similar to an "effective" Reynolds number increase. Although the present results pertaining to mean flow quantities support this assertion, it will be shown

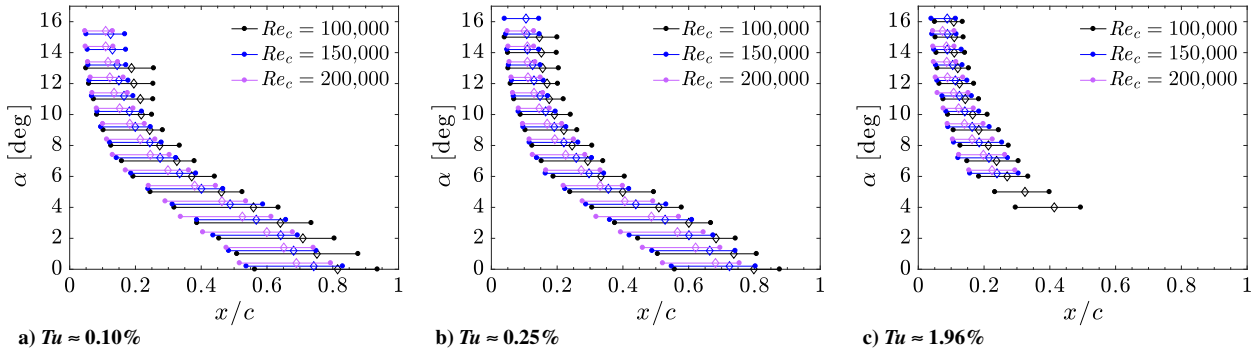

a) $Tu \approx 0.10\%$ b) $Tu \approx 0.25\%$ c) $Tu \approx 1.96\%$

Fig. 12 Effect of Reynolds number on mean bubble topology. Filled circles represent mean separation and reattachment locations. Diamond markers represent mean transition. Plots at equal angles of attack are offset slightly in the vertical direction for clarity. Uncertainties are approximately equal to the width of the diamond markers.

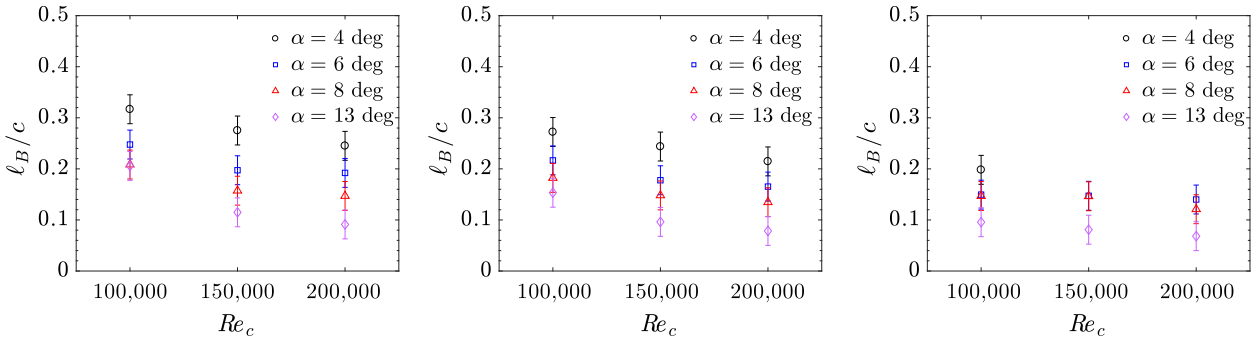

a) $Tu \approx 0.10\%$ b) $Tu \approx 0.25\%$ c) $Tu \approx 1.96\%$

Fig. 13 Effect of Reynolds number on mean bubble length.

in the next section that turbulence intensity and Reynolds number effects on transition characteristics differ quite significantly.

D. Separated Shear Layer Transition

The results presented in the previous sections indicate that the effect of elevated freestream turbulence intensity on airfoil performance and the underlying changes in the location and length of the separation bubble are related to the movement of the mean transition location (e.g., Fig. 8). Thus, the associated changes in transition characteristics are asserted in this section using time-resolved surface pressure measurements. It has been demonstrated in a number of previous investigations that characteristics of separated shear layer disturbances such as dominant frequencies and growth rates can be estimated from measured surface pressure fluctuations [41,42,45–47]. The relevant methodology for laminar separation bubbles is introduced and validated in [41,42], and the same approach is used in the present study.

Streamwise distributions of the rms of fluctuating surface pressures for increasing levels of Tu are presented in Fig. 14 for $\alpha = 4$ and 8 deg, being representative of low and prestall angles, respectively. Downstream of separation, rapid amplification of surface pressure fluctuations is observed, reflective of the amplification of perturbations in the separated shear layer [41]. As seen in Fig. 14, the pressure fluctuations attain maximum amplitudes just downstream of the mean transition location, and increasing Tu leads to an upstream shift in the streamwise location of the maxima, which follows the upstream movement of the mean transition location (Fig. 8). On the average, this is also accompanied by a decrease in the magnitude of maximum surface pressure fluctuations. This decrease is ascribed primarily to the reduction in the magnitude of vertical velocity fluctuations in the separated shear layer due to the increased influence of the wall for smaller separation bubbles [48].

Surface pressure fluctuation data can be used to estimate spatial amplification factors of shear layer disturbances as $\sigma = \ln(\Delta p'/q_0)/(\Delta x/c)$ [9,41]. The maxima of these spatial amplification factors are presented in Fig. 15. For a given Tu level, the amplification rates increase with increasing angle of attack, which explains the associated decrease in the separation bubble length (Fig. 9). In contrast, amplification rates decrease with increasing Tu for all angles of attack and Reynolds numbers investigated, thus implying that the bubble becomes more stable with increasing Tu. This is attributed to the decrease in the size of the separation bubble at higher Tu levels. A similar observation is reported by Dovgal et al. [49], who used analytic velocity profiles to show that stability in separated shear layers increases with decreasing distance to the wall. Decreased disturbance growth rates have also been observed in separation bubble studies with imposed mean flow deformations, both experimentally [48] and numerically [50]. The implication here is that the upstream shift in the location of mean transition at higher levels of Tu (Fig. 8) is solely the result of the increase in initial disturbance amplitude.

The effect of Re_c on maximum disturbance amplification rates is depicted in Fig. 16 for three levels of Tu. Here, $\sigma_{\max}$ increases with increasing Re_c, a trend that has been previously reported in a low-disturbance environment [9]. This result highlights a key difference between the effects of Re_c and Tu on separation bubble development. Although increasing either Re_c or Tu at a given angle of attack leads to a reduction in bubble size through the upstream advancement of mean transition, the former achieves this by decreasing flow stability (i.e., increasing amplification rates), whereas the latter has the opposite effect on stability, and the advancement of transition is the result of the increase in the initial amplitude of perturbations. Therefore, although there is an "effective" analogy between the two parameters with respect to their influence on mean bubble size and position [10], the underlying separated shear layer transition characteristics differ significantly. Similar observations have recently been made for separation bubbles formed over a flat plate [51].

It is instructive to consider the effect of elevated Tu levels on the frequency content of the shear layer disturbances. Spectra of the fluctuating surface pressures are computed using Welch's method [40], with a resulting frequency resolution of 2.4 Hz. The results are illustrated in Fig. 17 for $\alpha = 4$ and 8 deg at $Re_c = 100{,}000$.

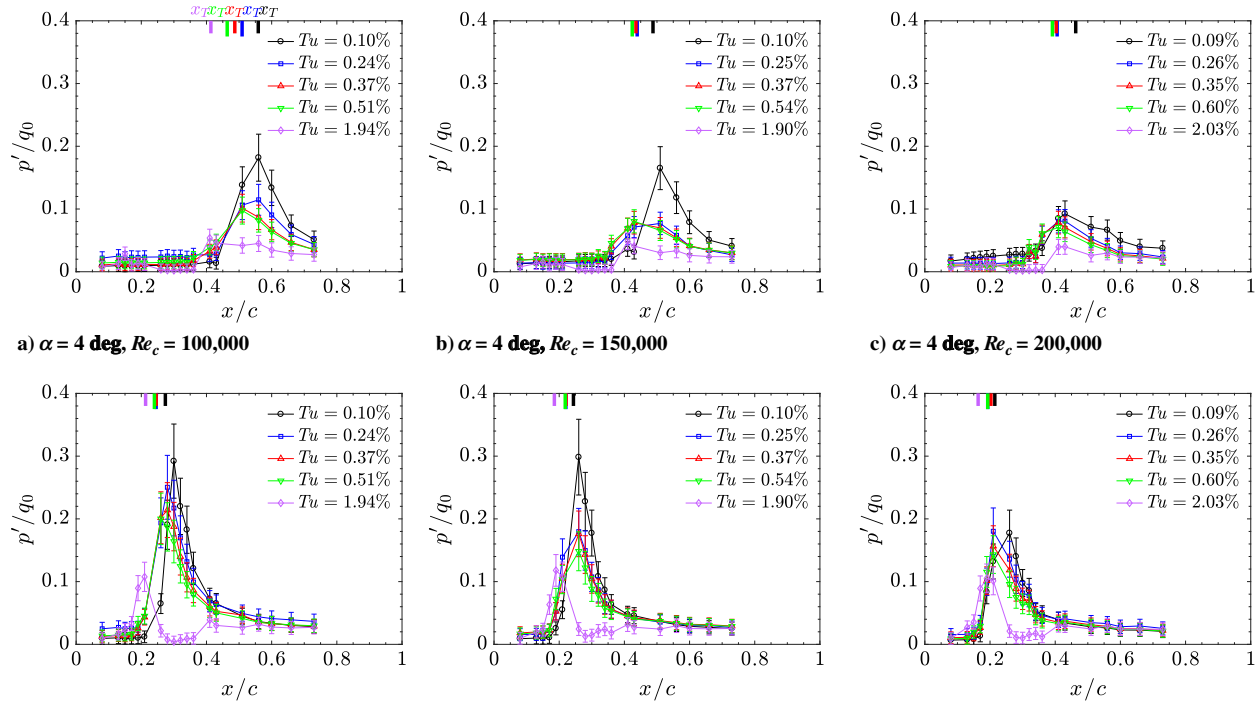

a) $\alpha = 4$ deg, $Re_c = 100{,}000$ b) $\alpha = 4$ deg, $Re_c = 150{,}000$ c) $\alpha = 4$ deg, $Re_c = 200{,}000$

d) $\alpha = 8$ deg, $Re_c = 100{,}000$ e) $\alpha = 8$ deg, $Re_c = 150{,}000$ f) $\alpha = 8$ deg, $Re_c = 200{,}000$

Fig. 14 Distributions of the rms of fluctuating surface pressure. Thick lines, colored according to the legend, indicate mean transition points.

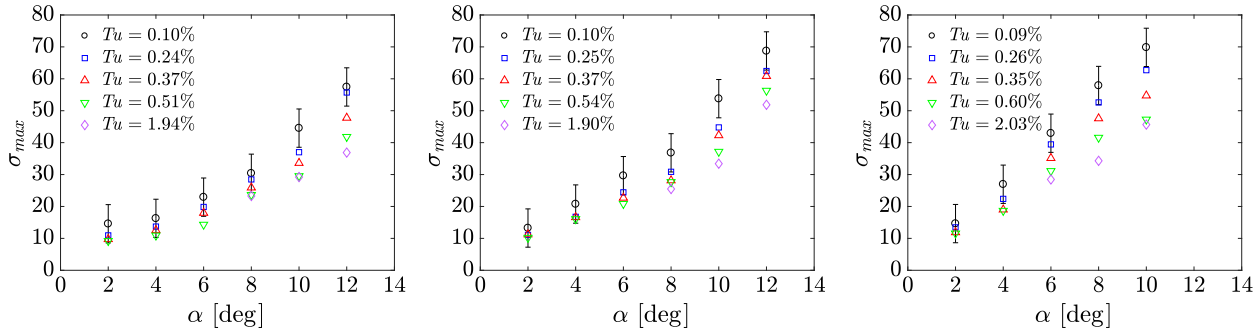

a) $Re_c = 100{,}000$ b) $Re_c = 150{,}000$ c) $Re_c = 200{,}000$

Fig. 15 Maximum spatial amplification factors.

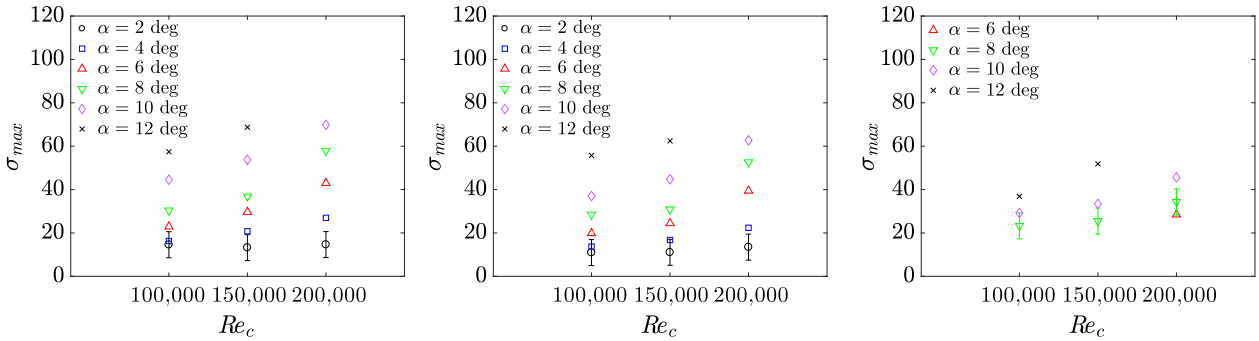

a) $Tu \approx 0.10\%$ b) $Tu \approx 0.25\%$ c) $Tu \approx 1.96\%$

Fig. 16 Effect of Reynolds number on maximum spatial amplification rates.

The spectra show that downstream of mean separation, disturbances are amplified within a band of frequencies Δf, centered on some central frequency f_0. Downstream of mean transition, the energy content is redistributed to a broader range of frequencies, whereas beyond mean reattachment, the spectra resemble those of a typical turbulent flow. As the level of Tu is increased, the detectable band of amplified frequencies broadens. This broadening is a result of the more significant energy content present across the relevant frequencies in the freestream (Fig. 3), which leads to earlier detectable amplitudes of fluctuations in the separated shear layer over a broader range of frequencies.

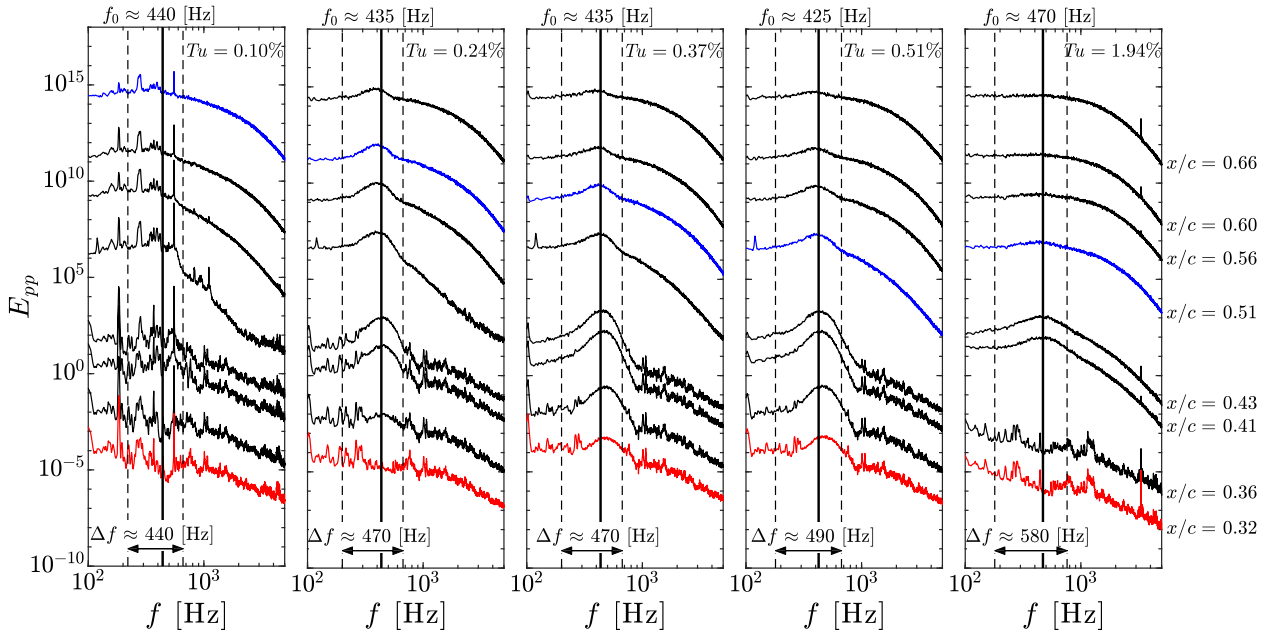

a) α = 4 deg

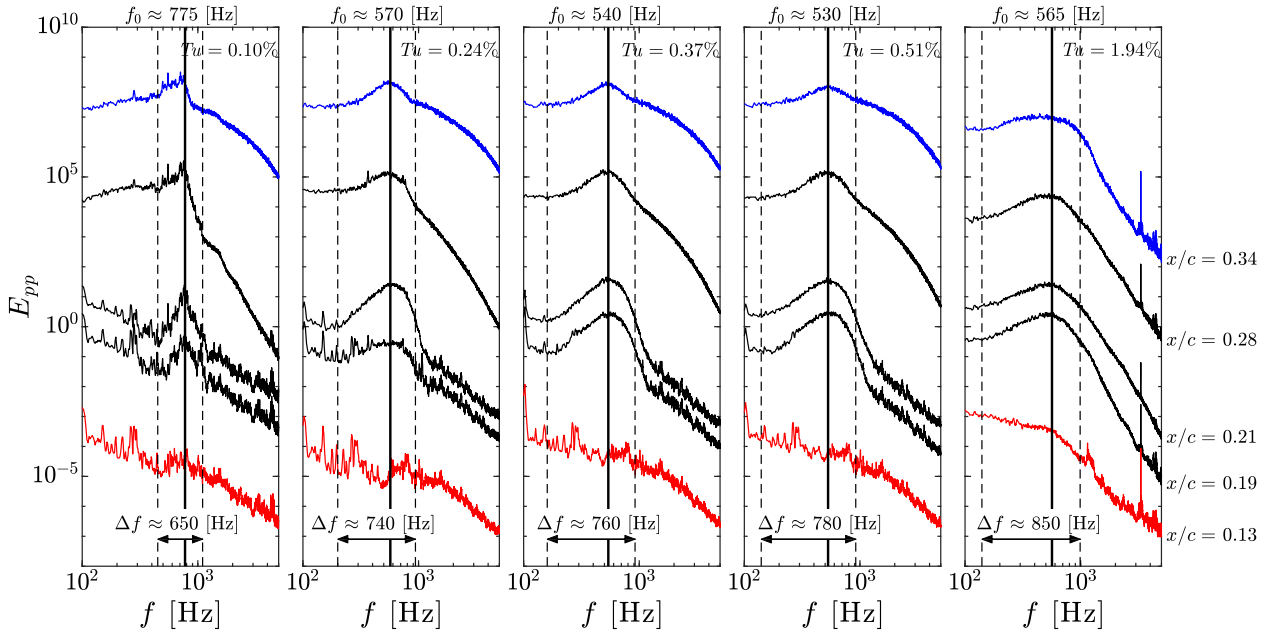

b) α = 8 deg

Fig. 17 Spectra of fluctuating surface pressures for $Re_c = 100{,}000$. All spectra are normalized by the total energy and stepped by an order of magnitude proportional to their chordwise position. Red and blue spectra indicate the approximate locations of mean separation and reattachment, respectively.

The central frequencies of amplified disturbances are estimated for all the cases examined, with the results summarized in Fig. 18. For a given level of Tu, the central frequency increases with increases in either angle of attack or Reynolds number, agreeing with the findings of Boutilier and Yarusevych [9]. At low angles of attack ($\alpha \leq 4$ deg), the central disturbance frequency does not change significantly for $Tu \lesssim 0.60\%$ despite the large changes in mean bubble topology (Fig. 9) and notable decreases in $\sigma_{\max}$ (Fig. 15). This trend is consistent with the decreased influence of mean flow deformation on the frequency of the most amplified perturbations as compared with the effect on growth rates as reported in [48,50]. At prestall angles of attack, f_0 initially decreases when the turbulence intensity is increased above the baseline level, followed by an increase in f_0 with further increases to Tu. These variations in the frequency of the most amplified perturbations become more significant with increasing angle of attack. The initial decrease in the frequency of the most amplified perturbations with increasing Tu level is in line with the expected moderate decrease due to the reduction in the size of the bubble [48,50]. However, the following increase in the most amplified frequency at high freestream turbulence levels ($Tu \geq 0.5\%$) does not conform to the trend expected from linear stability considerations [48,50], thus revealing a change in transition characteristics at high levels of Tu and hinting at a possible change in the nature of the transition process. In a simulation of a separation bubble induced on a flat plate at similarly high Tu levels, McAuliffe and Yaras [22] observed the formation of streamwise oriented streaks in the separated shear layer, which significantly altered the shear layer transition process. Similar changes have also been observed in flat plate boundary-layer transition under high levels of Tu [52–54], and it is speculated that similar streaks form in the present investigation at high levels of Tu ($Tu \geq 0.5\%$) and lead to the observed changes in central disturbance frequency. Thus, at sufficiently high levels of Tu,

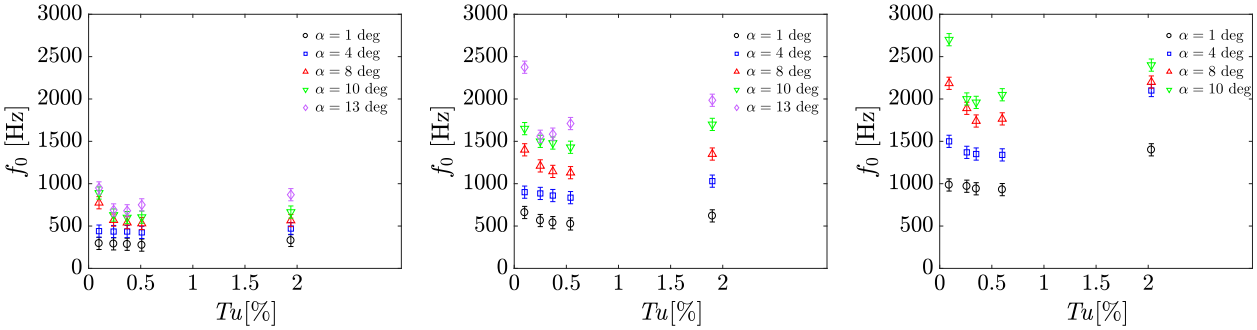

a) Re_c = 100,000 b) Re_c = 150,000 c) Re_c = 200,000

Fig. 18 Central disturbance frequencies.

transition is expected to occur before separation, eliminating the laminar separation bubble altogether. Although the associated critical values of Tu are expected to depend significantly on a given airfoil profile, its orientation, and Reynolds number, Mayle [55] provides an estimate for critical Tu levels at $Tu \approx 5\%$.

IV. Conclusions

The effects of freestream turbulence intensity on laminar separation bubbles forming over the suction side of an airfoil were investigated experimentally for angles of attack between 0 and 20 deg, chord Reynolds numbers between 100,000 and 200,000, and freestream turbulence intensities between 0.09 and 2.03%. Experiments were performed in a wind-tunnel facility, with mean and fluctuating surface pressure measurements used to characterize the mean bubble topology and the development of shear layer disturbances, respectively.

The results show that increasing the level of freestream turbulence intensity leads to a reduction in separation bubble length, which is caused primarily by an upstream shift in the locations of mean transition and, as a result, mean reattachment. At low angles of attack, the reduction in bubble length slightly reduces lift, whereas at larger angles of attack, this leads to increased lift and delayed stall. The main factors in determining the associated changes in airfoil lift are shown to be the size of the separation bubble and its proximity to the suction peak. Specifically, the reduction in bubble size due to elevated turbulence intensity is shown to alleviate the loss of suction when a separation bubble forms near the suction peak. At higher chord Reynolds numbers, the effect of increasing turbulence intensity is reduced, because increasing the Reynolds number also leads to similar changes in the size of a separation bubble. The effects of freestream turbulence intensity and Reynolds number on mean flow development are shown to be similar; however, the underlying changes in separated shear layer transition differ substantially.

Through the analysis of fluctuating surface pressures, it is demonstrated that the shear layer disturbances reach maximum values earlier upstream at higher levels of turbulence intensity, leading to the upstream shift in mean transition. The results demonstrate that spatial amplification rates of disturbances in the separated shear layer are reduced at higher turbulence intensity levels, which is attributed to the reduction in bubble size. In spite of the increased stability of the shear layer, the upstream shift in mean transition is achieved through the increase in initial disturbance amplitude with increasing freestream turbulence level. In contrast, the decrease in the size of the separation bubble achieved through increasing Reynolds number is due to the increase in spatial amplification rates in the shear layer.

Frequency spectra of the pressure fluctuations show that, as the turbulence intensity is increased, the frequency range associated with significant perturbations in the shear layer broadens as a result of the broader band of spectral energy present in the freestream. An initial increase in freestream turbulence intensities to moderate values ($Tu \leq 0.5\%$) leads to a decrease in the central disturbance frequency, expected from flow stability considerations reported in recent studies on laminar separation bubbles. In contrast, notable increases in central disturbance frequency are observed at higher levels of freestream turbulence intensity, which also suppress separation bubbles at lower angles of attack. It is speculated that this is attributed to the onset of bypass transition in the boundary layer upstream of separation.

Acknowledgments

The authors gratefully acknowledge the Natural Sciences and Engineering Research Council of Canada and Bombardier Aerospace for funding this work.

References

[1] Carmichael, B. H., "Low Reynolds Number Airfoil Survey, Volume 1," NASA CR-165803-VOL-1, 1981.

[2] Lissaman, P. B. S., "Low-Reynolds-Number Airfoils," *Annual Review of Fluid Mechanics*, Vol. 15, No. 1, 1983, pp. 223–239. doi:10.1146/annurev.fl.15.010183.001255

[3] Roberts, W. B., "The Effect of Reynolds Number and Laminar Separation on Axial Cascade Performance," *Journal of Engineering for Power*, Vol. 97, No. 2, 1975, pp. 261–273. doi:10.1115/1.3445978

[4] Mueller, T. J., "The Influence of Laminar Separation and Transition on Low Reynolds Number Airfoil Hysteresis," *Journal of Aircraft*, Vol. 22, No. 9, 1985, pp. 763–770. doi:10.2514/3.45199

[5] Mueller, T. J., and DeLaurier, J. D., "Aerodynamics of Small Vehicles," *Annual Review of Fluid Mechanics*, Vol. 35, No. 1, 2003, pp. 89–111. doi:10.1146/annurev.fluid.35.101101.161102

[6] Tani, I., "Low-Speed Flows Involving Bubble Separations," *Progress in Aerospace Sciences*, Vol. 5, 1964, pp. 70–103. doi:10.1016/0376-0421(64)90004-1

[7] Gaster, M., "The Structure and Behaviour of Laminar Separation Bubbles," Aeronautical Research Council, Reports and Memoranda No. 3595, London, 1967.

[8] McCullough, G. B., and Gault, D. E., "Examples of Three Representative Types of Airfoil-Section Stall at Low Speed," NACA Technical Rept. 2502, 1951.

[9] Boutilier, M. S., and Yarusevych, S., "Parametric Study of Separation and Transition Characteristics over an Airfoil at Low Reynolds Numbers," *Experiments in Fluids*, Vol. 52, No. 6, 2012, pp. 1491–1506. doi:10.1007/s00348-012-1270-z

[10] O'Meara, M. M., and Mueller, T. J., "Laminar Separation Bubble Characteristics on an Airfoil at Low Reynolds Numbers," *AIAA Journal*, Vol. 25, No. 8, 1987, pp. 1033–1041. doi:10.2514/3.9739

[11] Burgmann, S., and Schröder, W., "Investigation of the Vortex Induced Unsteadiness of a Separation Bubble via Time-Resolved and Scanning PIV Measurements," *Experiments in Fluids*, Vol. 45, No. 4, 2008, pp. 675–691. doi:10.1007/s00348-008-0548-7

[12] Hain, R., Kähler, C., and Radespiel, R., "Dynamics of Laminar Separation Bubbles at Low-Reynolds-Number Aerofoils," *Journal of Fluid Mechanics*, Vol. 630, July 2009, pp. 129–153. doi:10.1017/S0022112009006661

[13] Yarusevych, S., Sullivan, P. E., and Kawall, J. G., "On Vortex Shedding from an Airfoil in Low-Reynolds-Number Flows," *Journal of Fluid Mechanics*, Vol. 632, Aug. 2009, pp. 245–271. doi:10.1017/S0022112009007058

[14] Pauley, L. L., Moin, P., and Reynolds, W. C., "The Structure of Two-Dimensional Separation," *Journal of Fluid Mechanics*, Vol. 220, Nov. 1990, pp. 397–411.
doi:10.1017/S0022112090003317

[15] Watmuff, J. H., "Evolution of a Wave Packet into Vortex Loops in a Laminar Separation Bubble," *Journal of Fluid Mechanics*, Vol. 397, Oct. 1999, pp. 119–169.
doi:10.1017/S0022112099006138

[16] Marxen, O., Lang, M., Rist, U., and Wagner, S., "A Combined Experimental/Numerical Study of Unsteady Phenomena in a Laminar Separation Bubble," *Flow, Turbulence and Combustion*, Vol. 71, No. 1, 2003, pp. 133–146.
doi:10.1023/B:APPL.0000014928.69394.50

[17] Diwan, S. S., and Ramesh, O. N., "On the Origin of the Inflectional Instability of a Laminar Separation Bubble," *Journal of Fluid Mechanics*, Vol. 629, June 2009, pp. 263–298.
doi:10.1017/S002211200900634X

[18] Boutilier, M. S., and Yarusevych, S., "Separated Shear Layer Transition over an Airfoil at a Low Reynolds Number," *Physics of Fluids*, Vol. 24, No. 8, 2012, Paper 084105.
doi:10.1063/1.4744989

[19] Kurelek, J. W., Lambert, A. R., and Yarusevych, S., "Coherent Structures in the Transition Process of a Laminar Separation Bubble," *AIAA Journal*, Vol. 54, No. 8, 2016, pp. 2295–2309.
doi:10.2514/1.J054820

[20] Rist, U., and Maucher, U., "Investigations of Time-Growing Instabilities in Laminar Separation Bubbles," *European Journal of Mechanics-B/Fluids*, Vol. 21, No. 5, 2002, pp. 495–509.
doi:10.1016/S0997-7546(02)01205-0

[21] Jones, L. E., Sandberg, R. D., and Sandham, N. D., "Stability and Receptivity Characteristics of a Laminar Separation Bubble on an Aerofoil," *Journal of Fluid Mechanics*, Vol. 648, April 2010, pp. 257–296.
doi:10.1017/S0022112009993089

[22] McAuliffe, B. R., and Yaras, M. I., "Transition Mechanisms in Separation Bubbles Under Low- and Elevated-Freestream Turbulence," *Journal of Turbomachinery*, Vol. 132, No. 1, 2010, Paper 011004.
doi:10.1115/1.2812949

[23] Brinkerhoff, J. R., and Yaras, M. I., "Interaction of Viscous and Inviscid Instability Modes in Separation-Bubble Transition," *Physics of Fluids*, Vol. 23, No. 12, 2011, Paper 124102.
doi:10.1063/1.3666844

[24] Saric, W. S., Reed, H. L., and Kerschen, E. J., "Boundary-Layer Receptivity to Freestream Disturbances," *Annual Review of Fluid Mechanics*, Vol. 34, No. 1, 2002, pp. 291–319.
doi:10.1146/annurev.fluid.34.082701.161921

[25] Boiko, A. V., Grek, G. R., Dovgal, A. V., Kozlov, V. V., and Dowling, D. R., *Origin of Turbulence in Near-Wall Flows*, Vol. 56, 1st ed., Springer–Verlag, New York, 2003, pp. 93–95.

[26] Jones, L. E., Sandberg, R. D., and Sandham, N. D., "Direct Numerical Simulations of Forced and Unforced Separation Bubbles on an Airfoil at Incidence," *Journal of Fluid Mechanics*, Vol. 602, May 2008, pp. 175–207.
doi:10.1017/S0022112008000864

[27] Marxen, O., Lang, M., and Rist, U., "Vortex Formation and Vortex Breakup in a Laminar Separation Bubble," *Journal of Fluid Mechanics*, Vol. 728, Aug. 2013, pp. 58–90.
doi:10.1017/jfm.2013.222

[28] Olson, D. A., Katz, A. W., Naguib, A. M., Koochesfahani, M. M., Rizzetta, D. P., and Visbal, M. R., "On the Challenges in Experimental Characterization of Flow Separation over Airfoils at Low Reynolds Number," *Experiments in Fluids*, Vol. 54, No. 2, 2013, pp. 1470–1480.
doi:10.1007/s00348-013-1470-1

[29] Lengani, D., and Simoni, D., "Recognition of Coherent Structures in the Boundary Layer of a Low-Pressure-Turbine Blade for Different Free-Stream Turbulence Intensity Levels," *International Journal of Heat and Fluid Flow*, Vol. 54, Aug. 2015, pp. 1–13.
doi:10.1016/j.ijheatfluidflow.2015.04.003

[30] Mueller, T. J., Conigliaro, P., and Jansen, B. J., "The Influence of Free-Stream Disturbances on Low Reynolds Number Airfoil Experiments," *Experiments in Fluids*, Vol. 1, No. 1, 1983, pp. 3–14.
doi:10.1007/BF00282261

[31] Cao, N., Ting, D. S.-K., and Carriveau, R., "The Performance of a High-Lift Airfoil in Turbulent Wind," *Wind Engineering*, Vol. 35, No. 2, 2011, pp. 179–196.
doi:10.1260/0309-524X.35.2.179

[32] Mueller, T. J., "Aerodynamic Measurements at Low Reynolds Numbers for Fixed Wing Micro-Air Vehicles," Defense Technical Information Center Technical Rept. ADP010760, 1999.

[33] Ol, M. V., McAuliffe, B. R., Hanff, E. S., Scholz, U., and Kähler, C., "Comparison of Laminar Separation Bubble Measurements on a Low Reynolds Number Airfoil in Three Facilities," *35th AIAA Fluid Dynamics Conference and Exhibit*, AIAA Paper 2005-5149, 2005.

[34] Hillier, R., and Cherry, N. J., "The Effects of Stream Turbulence on Separation Bubbles," *Journal of Wind Engineering and Industrial Aerodynamics*, Vol. 8, No. 1, 1981, pp. 49–58.
doi:10.1016/0167-6105(81)90007-6

[35] Roach, P. E., "The Generation of Nearly Isotropic Turbulence by Means of Grids," *International Journal of Heat and Fluid Flow*, Vol. 8, No. 2, 1987, pp. 82–92.
doi:10.1016/0142-727X(87)90001-4

[36] Comte-Bellot, G., and Corrsin, S., "The Use of a Contraction to Improve the Isotropy of Grid-Generated Turbulence," *Journal of Fluid Mechanics*, Vol. 25, No. 4, 1966, pp. 657–682.
doi:10.1017/S0022112066000338

[37] Laws, E. M., and Livesey, J. L., "Flow Through Screens," *Annual Review of Fluid Mechanics*, Vol. 10, No. 1, 1978, pp. 247–266.
doi:10.1146/annurev.fl.10.010178.001335

[38] Batchelor, G. K., and Townsend, A., "Decay of Isotropic Turbulence in the Initial Period," *Philosophical Transactions of the Royal Society of London, Series A: Mathematical and Physical Sciences*, Vol. 193, No. 1035, 1948, pp. 539–558.
doi:10.1098/rspa.1948.0061

[39] Taylor, G., "The Spectrum of Turbulence," *Philosophical Transactions of the Royal Society of London, Series A: Mathematical and Physical Sciences*, Vol. 164, No. 919, 1937, pp. 476–490.

[40] Welch, P. D., "The Use of Fast Fourier Transform for the Estimation of Power Spectra: A Method Based on Time Averaging over Short, Modified Periodograms," *IEEE Transactions on Audio and Electroacoustics*, Vol. 15, No. 2, 1967, pp. 70–73.
doi:10.1109/TAU.1967.1161901

[41] Gerakopulos, R., and Yarusevych, S., "Novel Time-Resolved Pressure Measurements on an Airfoil at a Low Reynolds Number," *AIAA Journal*, Vol. 50, No. 5, 2012, pp. 1189–1200.
doi:10.2514/1.J051472

[42] Boutilier, M. S., and Yarusevych, S., "Effects of End Plates and Blockage on Low-Reynolds-Number Flows over Airfoils," *AIAA Journal*, Vol. 50, No. 7, 2012, pp. 1547–1559.
doi:10.2514/1.J051469

[43] Timmer, W., "Two-Dimensional Low-Reynolds Number Wind Tunnel Results for Airfoil NACA 0018," *Wind Engineering*, Vol. 32, No. 6, 2008, pp. 525–537.
doi:10.1260/030952408787548848

[44] Gerakopulos, R., Boutilier, M. S., and Yarusevych, S., "Aerodynamic Characterization of a NACA 0018 Airfoil at Low Reynolds Numbers," *40th AIAA Fluid Dynamics Conference*, AIAA Paper 2010-4629, 2010.

[45] Mabey, D. G., "Analysis and Correlation of Data on Pressure Fluctuations in Separated Flow," *Journal of Aircraft*, Vol. 9, No. 9, 1972, pp. 642–645.
doi:10.2514/3.59053

[46] Paterson, R. W., Vogt, P. G., Fink, M. R., and Munch, C. L., "Vortex Noise of Isolated Airfoils," *Journal of Aircraft*, Vol. 10, No. 5, 1973, pp. 296–302.
doi:10.2514/3.60229

[47] Cherry, N. J., Hillier, R., and Latour, M. E. M. P., "Unsteady Measurements in a Separated and Reattaching Flow," *Journal of Fluid Mechanics*, Vol. 144, July 1984, pp. 13–46.
doi:10.1017/S002211208400149X

[48] Yarusevych, S., and Kotsonis, M., "Steady and Transient Response of a Laminar Separation Bubble to Controlled Disturbances," *Journal of Fluid Mechanics*, Vol. 813, Feb. 2017, pp. 955–990.
doi:10.1017/jfm.2016.848

[49] Dovgal, A. V., Kozlov, V. V., and Michalke, A., "Laminar Boundary Layer Separation: Instability and Associated Phenomena," *Progress in Aerospace Sciences*, Vol. 30, No. 1, 1994, pp. 61–94.
doi:10.1016/0376-0421(94)90003-5

[50] Marxen, O., and Rist, U., "Mean Flow Deformation in a Laminar Separation Bubble: Separation and Stability Characteristics," *Journal of Fluid Mechanics*, Vol. 660, Oct. 2010, pp. 37–54.
doi:10.1017/S0022112010001047

[51] Simoni, D., Lengani, D., Ubaldi, M., Zunino, P., and Dellacasagrande, M., "Inspection of the Dynamic Properties of Laminar Separation Bubbles: Free-Stream Turbulence Intensity Effects for Different Reynolds Numbers," *Experiments in Fluids*, Vol. 58, No. 6, 2017, p. 66.
doi:10.1007/s00348-017-2353-7

[52] Fransson, J. H. M., Matsubara, M., and Alfredsson, P. H., "Transition Induced by Free-Stream Turbulence," *Journal of Fluid Mechanics*, Vol. 527, March 2005, pp. 1–25. doi:10.1017/S0022112004002770

[53] Jacobs, R. G., and Durbin, P., "Simulations of Bypass Transition," *Journal of Fluid Mechanics*, Vol. 428, Feb. 2001, pp. 185–212. doi:10.1017/S0022112000002469

[54] Zaki, T. A., "From Streaks to Spots and on to Turbulence: Exploring the Dynamics of Boundary Layer Transition," *Flow, Turbulence and Combustion*, Vol. 91, No. 3, 2013, pp. 451–473. doi:10.1007/s10494-013-9502-8

[55] Mayle, R. E., "The Role of Laminar-Turbulent Transition in Gas Turbine Engines," *Journal of Turbomachinery*, Vol. 113, No. 4, 1991, pp. 509–537. doi:10.1115/1.2929110

F. N. Coton
Associate Editor